Adsorption of HCl on Single-Crystal α-Al_2O_3 (0001) Surface: A DFT Study

Saman Alavi,[†] Dan C. Sorescu,[‡,§] and Donald L. Thompson*[,†]

Department of Chemistry, Oklahoma State University, Stillwater, Oklahoma 74078, U.S. Department of Energy, National Energy Technology Laboratory, Pittsburgh, Pennsylvania 15236, and Department of Chemical and Petroleum Engineering, University of Pittsburgh, Pittsburgh, Pennsylvania 15261

Received: July 8, 2002; In Final Form: September 30, 2002

First principles calculations based on density functional theory (DFT) and the pseudopotential method have been used to study the adsorption of HCl on the basal plane of an α-Al_2O_3 crystal. The calculations accurately reproduce the energetic and structural properties of bulk alumina and of the α-Al_2O_3 (0001) surface. A 2 × 2 supercell slab model was used to study both the molecular and dissociative adsorption of HCl on the α-Al_2O_3 (0001) surface. Our calculations indicate that the dissociative configurations have adsorption energies that are at least 28 kcal/mol greater than the molecular configurations on the surface. Several ionic adsorption configurations have been investigated in which the proton is adsorbed on a nearest neighbor surface O-ion site (1−2 adsorption), or a next nearest neighbor surface O-site (1−4 adsorption). We have found that the highest binding energy corresponds to 1−2 adsorption. Analysis of the surface coverage effects shows that by increasing the coverage of 1−2 adsorbed HCl molecules to a full monolayer, the adsorption energy of each HCl decreases by about 10 kcal/mol as a result of repulsions between neighboring molecules. Implications of HCl binding to particles of α-Al_2O_3 released in the exhaust of the space shuttle booster rockets on the active chlorine-producing reaction in the stratosphere are discussed.

1. Introduction

The binding of proton-donating molecules, HA, to metal oxide surfaces plays an important role in many natural and technical processes.[1,2] The adsorbate attaches to the ionic Lewis acid metal ion site on the surface through A, its electron-rich, nonmetal end. Surface binding of water[3,4] and hydrogen chloride[5] on the α-Al_2O_3 surface are examples of such processes. Adsorption can be followed by dissociation of the HA bond with the transfer of the proton to different surface Lewis-base oxygen ion sites or its diffusion to other surface-adsorbed HA molecules.

The nature of binding of HCl to the (0001) basal plane of single crystals of α-Al_2O_3 has been studied by Elam et al.[5] with laser-induced thermal desorption (LITD) and temperature-programmed desorption (TPD) techniques. They observed that HCl surface coverage saturates at $\theta_{HCl} = 1.0 \times 10^{14}$ molecules/cm^2 at 298 K, which is roughly equivalent to one HCl molecule per five surface Al sites. The saturation coverage was found to be independent of HCl pressure in the range 0.0125 to 4 Torr.

Temperature-programmed desorption studies performed at different HCl exposures showed that the peak temperature of desorption T_p is independent of surface coverage and the desorption shows first-order kinetics.[6] This observation indicates that HCl exists as a single molecular unit prior to desorption which implies either an associative mechanism for desorption or a strong pairing of two separate desorbing components.[7] Studies of the change in T_p with heating rate give a value of the activation energy of $E_d = 20 \pm 1$ kcal/mol with a value of the collisional frequency of $\nu = 10^{10\pm1}$ s^{-1}. The large activation energy for desorption shows that the molecular precursor to HCl desorption is chemisorbed on the surface. If desorption occurred directly from a dissociative state that involves mobile Cl^- and H^+, second-order kinetics and thus coverage dependence for the TPD peak temperatures would be expected.

Elam et al.[5] exposed the α-Al_2O_3 surface to constant amounts of HCl and annealed it to different temperatures in the range 298 to 500 K. Temperature-programmed desorption gave rise to signals with maxima shifted to higher temperatures over the range of 375 to 650 K. This implies the presence on the surface of a range of "sites" with different adsorption energies on the surface. Kinetic modeling of the TPD experimental data[5] indicates that the adsorption energies of these binding sites range from 19 to 36 kcal/mol. In another experiment, Elam et al.[5] exposed an α-Al_2O_3 surface to varying amounts of HCl at a constant temperature of 298 K. Thermal programmed desorption studies of this surface indicate that the position of the maximum of the TPD curves does not change with HCl surface coverage. From this observation, Elam et al.[5] concluded that HCl populates the surface adsorption sites randomly, independent of the binding energy of the sites. They also concluded that surface diffusion among sites must be negligible, otherwise the HCl would diffuse to higher energy binding sites and positions of the maxima of the TPD peaks would shift to greater temperatures at higher coverages. The fact that HCl desorption is independent of the HCl coverage at constant temperature implies that HCl populates various adsorption sites randomly and there is no diffusion between sites.

There is indirect experimental evidence to suggest that HCl is ionized upon adsorption on the α-alumina surface. For example, infrared spectroscopy studies[8,9] show that the adsorption of HCl on the γ-alumina surface leads to the formation of a new type of OH infrared adsorption band with an extinction coefficient larger than the original OH bands present on the surface. This suggests a dissociative adsorption mode for HCl

* Corresponding author.
[†] Oklahoma State University.
[‡] National Energy Technology Laboratory.
[§] University of Pittsburgh.

10.1021/jp021559j CCC: $25.00
Published on Web 12/02/2002

on γ-Al_2O_3. Additionally, isotope labeling[3] and high-resolution electron-energy loss spectroscopy (HREELS) studies of H_2O on α-Al_2O_3 show dissociative adsorption.[10] Since it is also expected that HCl adsorbs dissociatively on the α-Al_2O_3 surface, the fact that desorption of HCl follows first-order kinetics implies that either desorption must be preceded by recombination of H^+ and Cl^- on the surface, or that there is strong pairing between these ions on the surface.[7]

The adsorption and desorption of water on α-Al_2O_3 in TPD and LITD experiments shows qualitative features similar to those of HCl adsorbed on α-Al_2O_3. The structural and kinetic aspects of binding and proton diffusion of H_2O on the α-Al_2O_3 surface have been addressed in a comprehensive theoretical study by Hass et al.[11] On the basis of ab initio (Car-Parrinello) molecular dynamics calculations performed using a 3×3 hexagonal supercell, they concluded that H_2O is initially molecularly adsorbed. The route to the 1−4 dissociation mechanism (vide infra) has an activation barrier that is about a third of the 1−2 dissociation and so it constitutes the dominant pathway of dissociation. The ionic states for both dissociative mechanisms are 9 to 10 kcal/mol more stable than the molecularly adsorbed state and so the molecularly adsorbed water will spontaneously dissociate on the surface.

A theoretical study based on matching the results of a frozen-core valence method to an all-electron Hartree−Fock calculation for associative and dissociative adsorption of HCl at Al and O sites on partially hydrated Al_2O_3 clusters has been reported.[12] This study concludes that, on a perfect Al−O site (with Al in a 5-coordinated octahedral site), the adsorption energy of associative and dissociative HCl adsorption are −32 and −37 kcal/mol, respectively. These values are larger than the corresponding adsorption energies calculated for H_2O at the same site (−18 and +39 kcal/mol). Theoretical studies[11,13] of water adsorbed on Al_2O_3 clusters show that adsorption of H_2O may lead to large relaxations in the structure of the cluster. Due to the unconstrained nature of the cluster model, these structural changes will not be representative for adsorption onto the oxide surface. It is expected that surface slab models with periodic boundary conditions will provide a more realistic description of the surface relaxations and adsorption process. Such calculations were performed in the present work with the aim of understanding the details of the adsorption of HCl on the alumina surface.

The most stable phase of aluminum oxide is α-Al_2O_3 (corundum). Unlike many nonstoichiometric hydrated aluminum oxides, solid α-Al_2O_3 has a well-determined structure that has been widely studied, both experimentally and theoretically. Furthermore, it constitutes a large fraction of the alumina particles in the booster rocket exhaust of the space shuttle where metallic aluminum is used in the solid fuel.[14] For these reasons the solid phase of α-Al_2O_3 was chosen for our HCl adsorption studies.

Solid α-Al_2O_3 crystallizes in the D_{3d}^6 (or $R\bar{3}C$) space group.[15,16] The rhombohedral unit cell contains two Al_2O_3 molecular units with the atoms placed at special positions *4c* (Al ions), and *6e* (O ions). At room temperature, the lattice constants of this unit cell are $a = 5.128$ Å and $\alpha = 55.333°$.[15] Alternatively, a hexagonal unit cell containing six Al_2O_3 units with the Al and O ions residing in the *12c* and *18e* special positions, respectively, can also be considered to represent the $R\bar{3}C$ space group. The experimentally determined room-temperature lattice cell constants for this unit cell are $a = 4.762$ Å and $c = 12.896$ Å.[15] The structural parameters and high-temperature annealing behavior of the (0001) basal plane of the hexagonal unit cell have been well characterized by low-energy electron diffraction (LEED), Auger electron spectroscopy, and atomic force microscopy methods.[17−19] This surface orientation was used for the adsorption studies performed in this work.

Several theoretical studies have focused on a description of the structural properties of bulk Al_2O_3 and its surfaces. For example, Streitz and Mintmire[20] have developed a variable charge potential energy function that reproduces many of the bulk and surface oxide properties of aluminum oxide. This potential has been used in extensive molecular dynamics simulations which model the oxide formation process of aluminum nanoparticles.[21] Ab initio calculations using density functional theory in the local density approximation (LDA) have also been used to calculate the structural,[22,23] electronic, and optical[23] properties of α-Al_2O_3.

In the present work, we focus on HCl adsorption on the α-Al_2O_3 (0001) surface. To avoid some of the shortcomings of the cluster models previously used in theoretical investigations,[13] we have employed surface slab calculations with full periodic boundary conditions in all directions. The computational method is detailed in Section 2. Validation of the theoretical method used to predict the structural and energetic properties of bulk and surface Al_2O_3 is described in Section 3, where we also present an analysis of various molecular and ionic adsorption models of HCl on the (0001) basal plane of α-Al_2O_3 and compare the calculated values to the available experimental or theoretical data. A discussion of the results follows in Section 4 where implications of the HCl bonding on the reactions of the stratospheric ozone cycle are discussed. The conclusions are given in Section 5.

2. Theoretical Methods

The calculations performed in this study were done using the ab initio total-energy and molecular dynamics program VASP (Vienna ab initio simulation program) and the ultra soft pseudopotential database contained therein.[24−26] This program evaluates the total energy of periodically repeating geometries based on density functional theory (DFT) and the pseudopotential approximation. In this case, the electron−ion interaction is described by fully nonlocal optimized ultra soft pseudopotentials (USPPs) similar to those introduced by Vanderbilt.[27,28] Such pseudopotentials allow the use of a considerably smaller plane wave cutoff energy than would be needed with standard norm-conserving pseudopotentials. Periodic boundary conditions are used, with the one-electron pseudo-orbitals expanded over a plane wave basis set. The expansion includes all plane waves with kinetic energy less than a predetermined cutoff energy E_{cut}; i.e., $\hbar^2 G_{cut}^2/2m < E_{cut}$, where $G_{cut} > |\mathbf{k} + \mathbf{G}|$, and $\mathbf{G}$ is the reciprocal lattice vector, m is the electronic mass, and $\mathbf{k}$ is one of the k-points used to sample the Brillouin zone. The k-points are obtained from the Monkhorst-Pack scheme.[29] The values of E_{cut} and the k-point grid are chosen to ensure the convergence of energies and structures.

Throughout this work the calculations have been done using the spin-polarized Perdew-Wang 91 (PW91) generalized gradient-corrected exchange-correlation functional.[30,31] The minimization of the electronic free energy is carried out using an efficient iterative matrix-diagonalization routine based on a sequential band-by-band residuum minimization method (RMM)[25,26] or, alternatively, based on preconditioned band-by-band conjugate-gradient (CG) minimization.[32] The optimization of different atomic configurations is based upon a conjugate-gradient minimization of the total energy.

The minimum energy paths between different minima were optimized by use of the nudged elastic band (NEB) method of Jónsson and co-workers.[33] In this approach, the reaction path is "discretized", with the discrete configurations, or images, between minima being connected by elastic springs to prevent the images from sliding to the minima in the optimization. In the NEB searches, either 4 or 8 images were employed between minima.

3. Results

A. Preliminary Tests for Bulk α-Al_2O_3. As a first test of the accuracy of our calculations, we have determined the lattice constants of a rhombohedral α-Al_2O_3 unit cell and the positions of the Al and O ions. These calculations were done with a 3 × 3 Monkhorst-Pack[29] grid of *k*-points and an energy cutoff of 450.0 eV.

The optimization of the bulk unit cell has been done using a two-step procedure. First we have determined the volume of the unit cell that minimizes the total energy. Then the lattice vectors have been optimized for the optimal volume determined at the first step. During this set of calculations the positions of the ions were allowed to relax to equilibrium.

At the lowest energy, the calculated rhombohedral unit parameters are $a_{calc} = 5.20$ Å, and $\alpha_{calc} = 55.252°$. For the hexagonal unit cell representation the corresponding values are $a = 4.83$ Å, and $c = 12.66$ Å. These data are within 2% of the experimental values[15] and are also close to the calculated values $a_{calc} = 5.123$ Å and $\alpha_{calc} = 55.20°$ obtained by Manassidis et al.[22] using DFT in the local density approximation. The positions of the Al and O ions were calculated to be $u(Al) = 0.3526$ and $u(O) = 0.5567$, which correspond with the experimental values of 0.352 and 0.556, respectively.[15]

From the dependence of the unit cell energy on the volume we have determined also the bulk modulus using the Murnaghan equation,[34]

$$E(V) = \frac{B_0}{B_0'} V \left[\frac{1}{B_0' - 1} \left(\frac{V_0}{V} \right)^{B_0'} + 1 \right] + C \qquad (1)$$

where V is the volume of the unit cell, V_0 the volume of the same unit cell at zero pressure, C is a constant,

$$B_0 = V \left(\frac{\partial^2 E}{\partial V^2} \right) \Big|_{V = V_0} = - V \left(\frac{\partial P}{\partial V} \right) \Big|_{V = V_0} \qquad (2)$$

is the bulk modulus of the solid at zero pressure, and $B_0' = dB_0/dP$ is the pressure derivative of the bulk modulus. The partial derivatives in eq 2 are taken at isothermal (T = const) conditions. On the basis of these equations we have obtained $B_0 = 2.23$ MPa, $B_0' = 3.62$, and $V_0 = 88.353$ Å^3. These values are in good agreement with the experimental result[35] of $B_0 = 2.54$ MPa and the previous DFT LDA results of Ching and Xu,[23] $B_0 = 2.42$ MPa, and $B_0' = 3.24$.

Additionally, the cohesive energy, E(cohesive), per Al_2O_3 unit for the rhombohedral unit cell was determined to be 32.13 eV by using the equation

$$E(\text{cohesive}) = {}^1/_2[E(2Al_2O_3) - 4E(Al) - 6E(O)] \qquad (3)$$

where $E(Al_2O_3)$ is the energy of the unit cell and E(Al) and E(O) are the energies of the separate Al and O atoms of the lattice, respectively. The calculated value of E(cohesive) differs by 1% from the experimental value of 31.8 eV.[36]

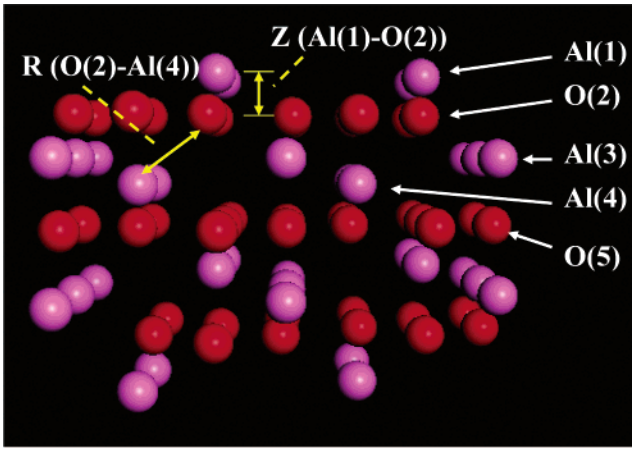

Figure 1. Side view of the unrelaxed nine-layer surface slab. This corresponds to a 2 × 2 supercell. The first five layers of the slab are labeled. The surface Al and O ions are under-coordinated. The pink spheres represent the Al ions and the red spheres the O ions.

B. Results of Surface Slab Model. Surface relaxation studies were done for the (0001) basal plane of α-Al_2O_3. In this case the surface has been modeled as a 2 × 2 supercell containing three layers of oxygen ions (36 ions) and six layers of Al ions (24 ions). The slab is terminated by Al ions and a vacuum layer of about 10 Å is used to separate the neighboring slabs in a direction perpendicular to the surface. The supercell vectors were chosen on the basis of the optimized values from the bulk calculations. A single Γ-point centered *k*-point was used in the surface calculations.

In the bulk solid, each Al ion is coordinated to four O ions, whereas each O ion is coordinated to six Al ions. In the unrelaxed structure the surface Al and O ions are under-coordinated with each having three and four neighbors, respectively. A side view of the layered structure of the unrelaxed 2 × 2 supercell is shown in Figure 1 together with the labels for the different ionic layers. Two examples of the notation used to describe the vertical separation between two neighbor layers of ions, $Z(Al_{(1)}-O_{(2)})$, and the distance between specific ions in these layers, $R(O_{(2)}-Al_{(4)})$, are given in this figure. The numerical values of these two length parameters are given in Table 1.

In the case of slab calculations, the atoms on the top and bottom sides of the slab model have been allowed to relax. A side view and top view of the relaxed structure are given in Figure 2a and 2b, respectively. The Al ions of the outermost surface layer relax into the outer layer of O ions, such that the distance between these layers decreases by as much as 97% relative to the unrelaxed distances. Considerable relaxation is seen for the middle layers as well. The percentage change of the vertical distance between layers as compared to the bulk solid phase is given in Table 1 along with a selection of bond lengths. The corresponding percent changes in the surface spacing determined in a previous DFT LDA study[11] and from an X-ray scattering experiment[37] are also given for comparison. Both our results as well as those obtained using the LDA method indicate a vertical relaxation for the outermost layer of Al ions of about −90% relative to the bulk structure. These values overestimate the corresponding vertical relaxation found experimentally of −52%.[37(a)] The nature of this large discrepancy has been discussed previously by Hass et al.[11] They indicated that experimentally it is difficult to prepare a hydrogen-free Al_2O_3 surface. They referenced the experimental work of Ahn and Rabalais[37(b)] who observed that even for annealing at temperatures as high as 1100 °C, hydrogen atoms were still

TABLE 1: Bond Lengths *R* (Å) and Distances between Adjacent Layers *Z* (Å) in the Bulk and in the Relaxed Surface Slab of α-Al_2O_3 from VASP Calculations, and Percentage Changes in Distances between Neighboring Layers in Going from the Bulk to the Surface Slab

bulk distances	length
R(Al−O)	1.88
R(Al′−O)	2.00
Z(Al−O)	0.84
Z(Al−Al′)	0.51

surface slab distances[a]	length	calculated % change present work	calculated % change Hass et al.[b]	expt[c]
$R(Al_{(1)}-O_{(2)})$	1.69			
$R(O_{(2)}-Al_{(3)})$	1.81			
$R(O_{(2)}-Al_{(4)})$	1.89			
$Z(Al_{(1)}-O_{(2)})$	0.02	−97	−2	−51
$Z(O_{(2)}-Al_{(3)})$	0.86	+2	+4	+16
$Z(Al_{(3)}-Al_{(4)})$	0.24	−53	−51	−29
$Z(Al_{(4)}-O_{(5)})$	1.07	+27	+24	+20

[a] The subscripts on the ion labels in the surface slab results refer to the number of the layer from which the ion originates, see Figure 1. [b] Hass et al., ref 11. [c] Guenard et al., ref 37(a).

abundant on the surface in large quantities. It is believed[11,37(b)] that the presence of hydrogen on the surface will cause significant changes in the surface relaxation.

The surface energy σ for the relaxed structure was calculated from the equation

$$\sigma = [E(\text{slab}) - E(\text{bulk})]/2S \quad (4)$$

where E(slab) = −435.544 eV is the energy of the relaxed slab and E(bulk) = −449.784 eV is the energy of the bulk sample having the same number of atoms and using the same *k*-point setting as that used for the slab. In eq 4, S represents the surface area and the factor of 2 in the denominator arises from the fact that we have allowed both the upper and lower layers of the slab to relax. The value of 1.42 J/m^2 obtained from our calculations compares favorably with previous data determined on the basis of DFT calculations,[22] σ = 1.76 J/m^2; or based on empirical potentials for α-Al_2O_3 (which include ionic interactions and two-body interactions between neighboring species): σ = 2.03 J/m^2 from ref 38 and σ = 2.97 J/m^2 from ref 39.

C. Tests for the Isolated HCl Molecule. The accuracy of the ultrasoft set of pseudopotentials used in this study has also been tested by calculations of the equilibrium and vibrational properties of the HCl molecule. These have been determined by placing an isolated HCl molecule in a cubic box of length 10 Å and calculating the variation of energy of the molecule as a function of the HCl bond distance. The equilibrium HCl bond length from these calculations was determined to be 1.290 Å. The variation of the total energy as a function of the HCl interatomic distance was fit with a Morse potential to determine the fundamental vibrational frequency of the HCl bond which was found to be 2890.1 cm^{-1}. These values reproduce well the experimental HCl bond length[40] of 1.2746 Å and vibrational frequency of 2885.9 cm^{-1}.[41]

As a final test, we have determined the atomization energy of HCl molecule using VASP. This value can be obtained from the equation

$$D^0 = E(\text{H}) + E(\text{Cl}) - E(\text{HCl}) - {}^1/_2 h\nu_0 \quad (5)$$

where D^0 is the atomization energy (bond dissociation energy), E(H) and E(Cl) are the calculated energies of the hydrogen and chlorine atoms, respectively, and E(HCl) is the energy of an isolated HCl molecule. The final term on the right side of eq 5 is the zero-point energy correction to the atomization energy. Substituting the calculated values for the atomization energy at 0 K, we obtain $D°$ = 4.5277 eV. The experimental value at 298 K is D^0_{298} = 4.4716 eV.[36]

The totality of these results indicate that the set of pseudopotentials and the computational methods we have used are able to provide a good description of both the bulk system and the bare surface as well as for the isolated molecules and the individual atomic species. These characteristics are required conditions for providing an accurate analysis of the interaction of the HCl molecule with the α-Al_2O_3(0001) surface.

D. Adsorption of HCl on the Al_2O_3(0001) Surface. The adsorption studies of HCl on the α-Al_2O_3(0001) surface were done using a 2 × 2 supercell with four Al surface ions. Both molecular and ionic dissociative modes of adsorption of HCl molecules have been considered. Due to the greater number of O anion sites than Al cation sites on the surface, at low coverages there are various surface oxygen sites where H^+ can attach. Consequently different separations for the dissociated H^+ from the Cl^-, labeled as the 1−2, and 1−4 adsorptions, were analyzed. Finally the effects upon the adsorption energies of different HCl coverages ranging from a half monolayer (ML) to a full ML have been studied. As the surface area of the 2 × 2 supercell used in our calculations is 80.563 Å^2, a full ML coverage is equivalent to 4.96 × 10^{14} molecules/cm^2. The adsorption energies calculated throughout this work were obtained using the equation

$$E(\text{adsorption}) = -[E(\text{slab} + \text{HCl}) - E(\text{slab}) - \text{N} \times E(\text{HCl})]/N \quad (6)$$

where N is the number of adsorbed HCl units on the surface slab, E(HCl) is the energy of the isolated HCl molecule at its equilibrium bond length, E(slab) is the total energy of the slab, and E(slab + HCl) is the total energy of the adsorbate/slab system.

D1. Molecular Adsorption of HCl. The molecular adsorption configurations of HCl were determined by optimizations in which the initial state was obtained by placing the Cl end of the HCl molecule above a surface Al ion with the HCl bond initially parallel to the surface. The HCl bond length was taken equal to that found in the gas phase. Two orientations for the HCl bond were considered. When a Cl atom is adsorbed onto an Al site (hereafter called Al_{ad}) the HCl bond can be either in an "eclipsed" orientation where it is directly oriented above a neighboring surface Al−O bond, or it is "staggered" between two surface Al−O bonds. The calculated adsorption energies for these two orientations are given in Table 2. These values differ by approximately 1 kcal/mol. Table 2 also gives the percent change of the distance between Al_{ad} ions and the second layer of O ions. It is found that the Al_{ad} ion attached to the Cl has moved outward compared to the bare surface (−54% relaxation relative to the bulk as compared to −97% in the bare surface), but the distance to the layer of surface O ions, $Z(Al_{ad}-O_{(2)})$, is still significantly smaller than Z(Al−O) in bulk alumina. Other structural modifications of the surface slab as a result of the molecular adsorption of HCl are given in Table 3.

D2. Ionic Adsorption of HCl. The ionic adsorption of HCl on the surface slab was modeled by placing Cl^- and H^+ at different vertical distances above a chosen pair of Al and O ions and allowing their positions to relax to the most stable configuration. In the initial configuration, the separation between

TABLE 2: The Adsorption Energies E_{ad} (kcal/mol) for Various Modes of Adsorption of HCl on a 2 × 2 Supercell, and the Percent Change in Spacing of Al_{ad} from the Second Layer of O Ions Relative to That of Bulk Alumina[a]

mode of adsorption	E_{ad} for HCl	% change in $Z(Al_{ad}-O_{(2)})$	E_{ad} for H_2O[b]	% change in $Z(Al_{ad}-O_{(2)})$
eclipsed molecular adsorption	11.7	−54%	23.3	−49%
staggered molecular adsorption	10.6	−57%		
1−2 ionic adsorption	43.7	−14%	33.2	−13%
1−4 ionic adsorption	39.9	−20%	32.5	−14%
1−2 ionic adsorption, two HCl units	43.3			
1−2 ionic adsorption, four HCl units	34.6			

[a] The corresponding geometric and energetic parameters for H_2O adsorption on the same surface from ref 11 are given for comparison. [b] Hass et al., ref 11.

TABLE 3: Representative Bond Lengths *R* (Å) for Various Adsorption Configurations of HCl on the α-Al_2O_3(0001) Surface[a]

bond distances[b]	length	length
Molecular adsorption	Eclipsed HCl	Staggered HCl
$R(Cl-Al_{ad})$	2.43	2.49
$R(H-Cl)$	1.40	1.30
$R(Al_{ad}-O_{ad})$	1.74	
$R(Al_{ad}-O_{(2)})$	1.69, 1.69	1.70, 1.71, 1.71
$R(O_{ad}-Al_{(3)})$	1.83	1.80
$R(O_{ad}-Al_{(4)})$	1.93	1.89
Ionic Adsorption	1−2 Ionic HCl	1−4 Ionic HCl
$R(Cl-Al_{ad})$	2.12	2.14
$R(H-O_{ad})$	0.98	0.98
$R(Al_{ad}-O_{ad})$	1.90	
$R(Al_{ad}-O_{(2)})$	1.74, 1.74	1.76, 1.78, 1.78
$R(O_{ad}-Al_{(3)})$	1.91	1.91
$R(O_{ad}-Al_{(4)})$	2.01	2.01
Multiple Ionic Adsorption	Two HCl units	Four HCl units
$R(Cl-Al_{ad})$	2.11	2.11
$R(H-O_{ad})$	0.98	1.98
$R(Al_{ad}-O_{ad})$	1.90	
$R(Al_{ad}-O_{(2)})$	1.75	

[a] For multiple adsorption of HCl the H^+ ions are attached to O ions adjacent to Al_{ad}. [b] The subscripts refer to the layers in the surface slab as shown in Figure 1.

Cl^- and H^+ is large (1.8 Å) such that the covalent bond between the two is effectively broken.

As mentioned previously, upon ionization H^+ can become attached to various surface oxygen ions. The oxygen attached to the H^+ is denoted as O_{ad}. In the 1−2 dissociation, the H^+ binds to one of the three nearest neighbor O ions of the Al_{ad}. These ions are spaced 1.689 Å apart and are marked with circles in Figure 2b. In 1−4 dissociation, the proton binds to one of the three next-nearest neighbor O ion sites. The distance of these O ions to the Al_{ad} is 3.135 Å and they are marked with squares in Figure 2b. The nomenclature of these dissociated states adopted in our work is similar to the one used previously by Hass et al.[11]

Each surface Al ion has three nearest neighbor O ions in the surface layer, which are related by a 3-fold axis of symmetry. For the 1−2 dissociation, these three O ions provide equivalent sites for the attachment of the H^+ upon its dissociation from Cl^-. The results of calculations for the adsorption energy and the corresponding geometric parameters are given in Tables 2 and 3, respectively. Figure 3 illustrates the configurations for the three possible 1−2 dissociation products.

Several geometric relaxations of the surface atoms take place as a result of dissociative chemisorption. By binding to the Cl^-, the coordination number of the Al_{ad} ion increases to four, which is the value of the coordination number of the Al ion in bulk α-Al_2O_3. This results in the outward relaxation of the Al_{ad} ion and an increase in its vertical separation from the layer of surface

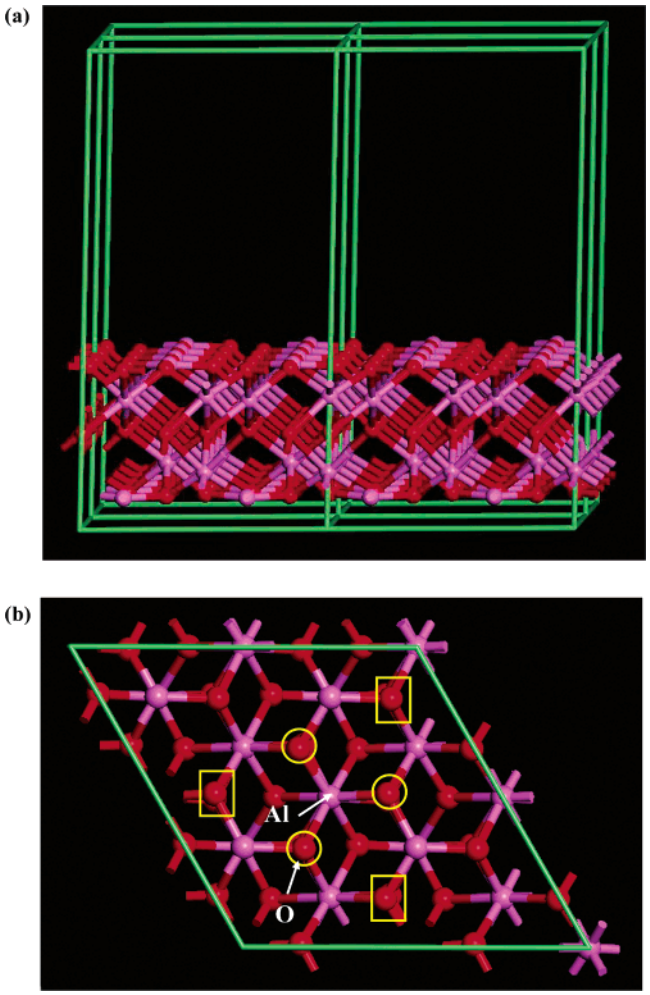

Figure 2. (a) Side view of the relaxed slab model used to simulate the Al_2O_3(0001) surface. The $Al_{(1)}$ layer of ions (from Figure 1) has relaxed into the topmost layer of oxygen ions. Structural information for these configurations is given in Table 1. The pink spheres represent the Al ions and the red spheres represent the O ions. (b) A top view of the relaxed α-alumina surface. A reference surface Al ion with its neighboring 1−2 O ions are shown by circles. Squares are superimposed on the 1−4 neighboring O ions. The nomenclature of the surface O ions is described in the text.

O ions. The vertical distance of Al_{ad} to the plane of $O_{(2)}$ ions is ∼0.6 Å compared to 0.02 Å in the bare surface. The O_{ad} is also pulled upward from the surface by ∼0.08 Å. The OH bond lengths on the surface (0.98 Å) are close to those of OH bonds in isolated molecules such as water (0.958 Å), but the $Al_{ad}-Cl$ bond is considerably shorter than that of the molecularly adsorbed state. The binding energies of the ionic configuration are considerably greater than the binding energies of molecularly adsorbed HCl with values in the range 40−44 kcal/mol.

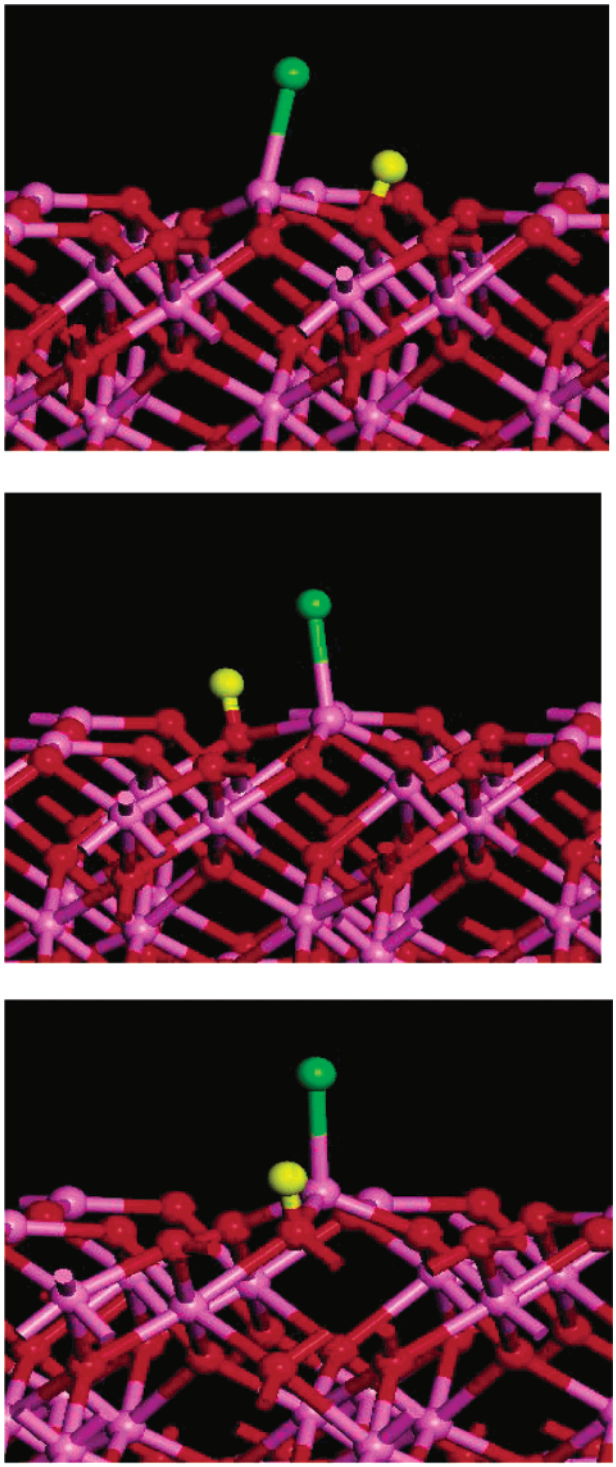

Figure 3. A side view of three possible 1−2 dissociative adsorption modes of HCl on the α-alumina surface. The considerable relaxation of the Al_{ad} ion away from the surface is seen in the side view. Structural parameters for these configurations are given in Table 3.

The distance between the Cl^- and H^+ ion pair is greater for the 1−4 dissociative adsorption, and the adsorption energy of the HCl unit is less than in 1−2 adsorption. In all cases, however, the dissociative adsorption energies are considerably larger than those for molecular adsorption. Relaxation patterns of the ions in the 1−4 adsorption are similar to those of 1−2 adsorption. In the 1−4 adsorption, the Al_{ad} ion also relaxes outward by a significant amount, approximately 0.5 Å.

The experimental surface coverage of the HCl on an Al_2O_3 surface is approximately equivalent to 1 HCl per 2 × 2 supercell. On a local scale, however, there is the possibility of clustering of the ionized HCl units. To study this effect, two HCl units were placed in a 2 × 2 supercell. The HCl molecules are both ionized with the H^+ and Cl^- in 1−2 proximity. The adsorption energy per H^+ and Cl^- ion pair for this configuration is given in Table 2. The adsorption energy is slightly less as a result of neighboring electrostatic repulsions between the ions compared to that for a single HCl on the surface. For the complete monolayer coverage of four HCl molecules per 2 × 2 supercell, the binding energy per HCl molecule shows a decrease of about 10 kcal/mol compared to single molecule 1−2 adsorption.

E. Energy Barriers to Proton Migration on the α-Alumina Surface. The energy profiles for the migration of H^+ from the molecularly adsorbed parent HCl upon ionization have been calculated using the nudged elastic band (NEB) method.[32] Also, the energy barrier to proton migration between the oxygen sites on the surface from a 1−2 to a 1−4 ionic configuration has been calculated.

The energy profile for the conversion of the staggered molecular adsorbed state to the 1−4 ionic state is shown in Figure 4. The structures corresponding to the initial, final, and one intermediate configuration are also shown in these figures. There is no energy barrier to proton transfer in this case. Similar results for the transformation of the eclipsed molecular adsorbed state to the 1−2 ionic state are shown in Figure 5. A very shallow intermediate region is observed in this case, but again there is no effective energy barrier to proton transfer. These two sets of results indicate that adsorption from the gas phase will lead directly to ionic adsorbed states.

The energy profile for the transfer of a proton from a 1−2 ionic state to a 1−4 ionic state is presented in Figure 6. The corresponding configurations for the initial, transition state, and the final configurations are also shown in this figure. Although the adsorption energies for the two ionic states are close to one another, 43.7 and 39.9 kcal/mol for the 1−2 and 1−4 forms, respectively, the energy barrier to transform from one ionic structure to the other is high (about 22 kcal/mol). It is therefore unlikely that proton transfer will occur between these ionic structures. The molecules will remain in the initial adsorption sites with different adsorption energies and thus not necessarily all occupy the lowest energy sites. This theoretical observation is in agreement with the experimental TPD studies which suggest that there is no transfer of the adsorbed molecules or ions between sites of different adsorption energy.[5]

4. Discussion

The results of this work are consistent with the experimental observations of Elam et al.[5] An adsorption energy of approximately 10 to 12 kcal/mol was calculated for molecular adsorption of a single HCl molecule on the supercell, whereas for ionic dissociative adsorption the calculations gave adsorption energies ranging from 40 to 44 kcal/mol, depending on the relative separation of the surface sites of Cl^- and H^+. The experimental saturation surface coverage of HCl on α-Al_2O_3 is approximately one adsorbed HCl molecule per five surface Al sites. The values given in Table 2 show that the surface binding energy decreases with increase of surface coverage. Local clustering will lead to a further spread in HCl binding energies. Additionally, the adsorption of HCl at the surface defective sites and steps, which were not considered in this work, will also lead to a even further spread of the adsorption energies. These many factors can explain the range of adsorption energies needed by Elam et al.[5] to explain the TPD data. All these factors contribute to the spread of the adsorption energies as determined by Elam et al.[5] in their TPD experiments.

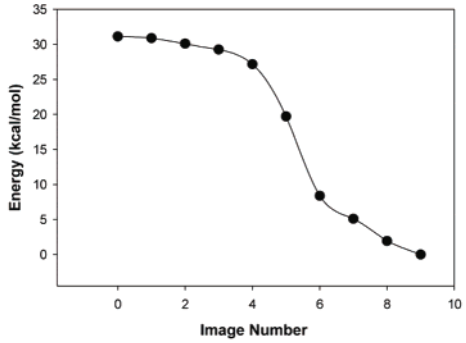

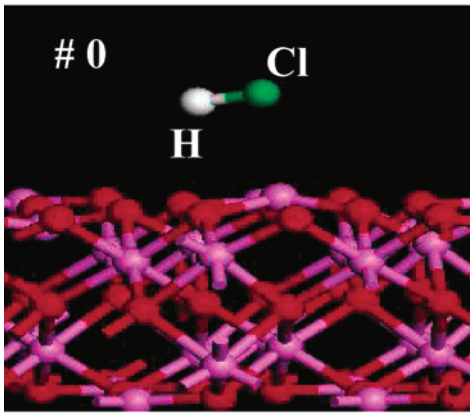

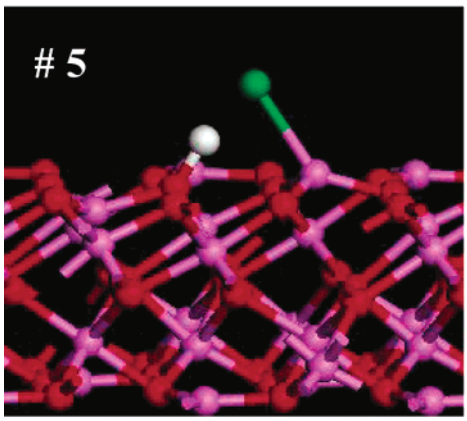

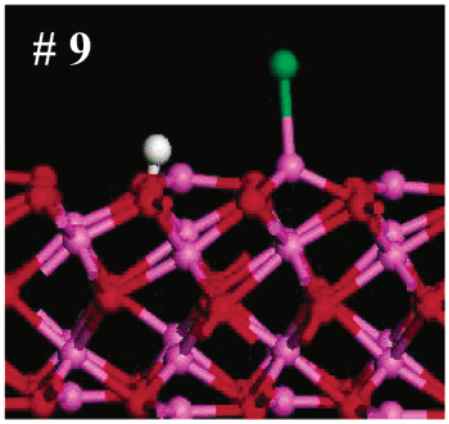

Figure 4. The energy profile for the conversion of the staggered molecular HCl to a 1−4 ionic HCl adsorbed on the α-Al_2O_3 surface. No activation barrier is predicted. Representative configurations indicating the conversion of the molecular to ionic HCl on the surface are also shown. The labels on these configurations correspond to the image number indicated in the potential profile.

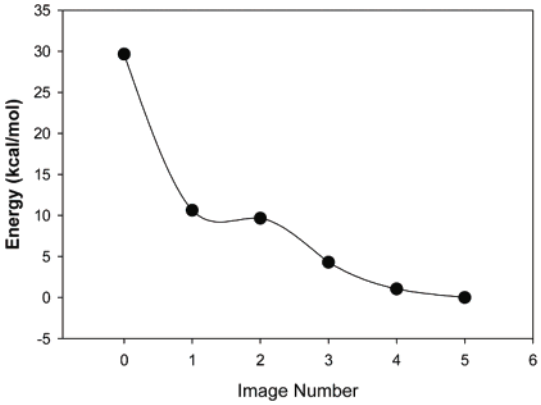

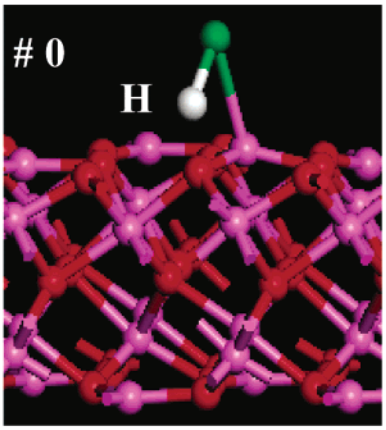

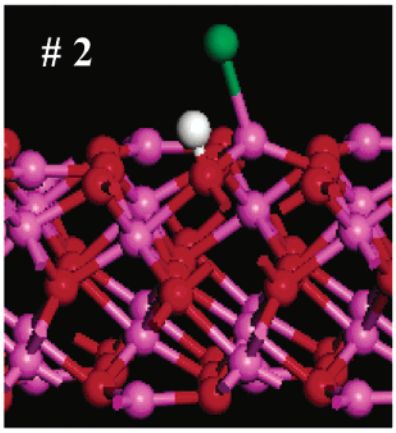

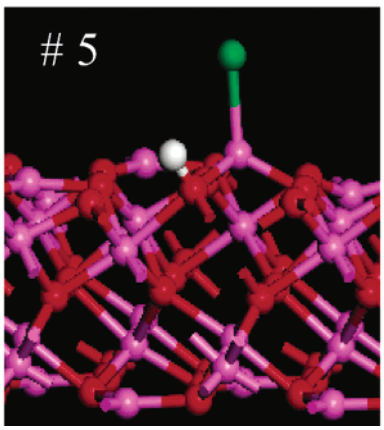

Figure 5. The energy profile for the conversion of the eclipsed molecular HCl to a 1−2 ionic HCl adsorbed on the α-Al_2O_3 surface. The energy profile shows a shallow minimum, but no effective activation barrier is predicted. The labels on the representative configurations correspond to the image number in the potential profile.

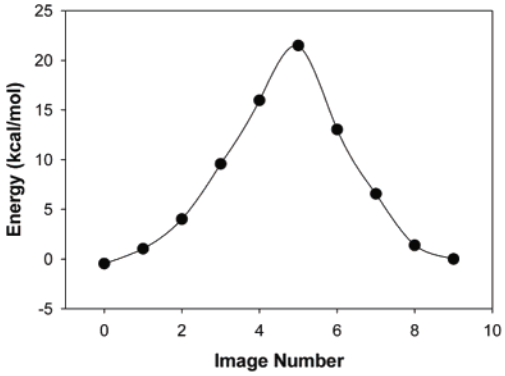

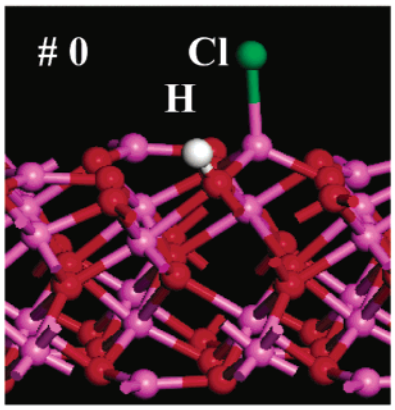

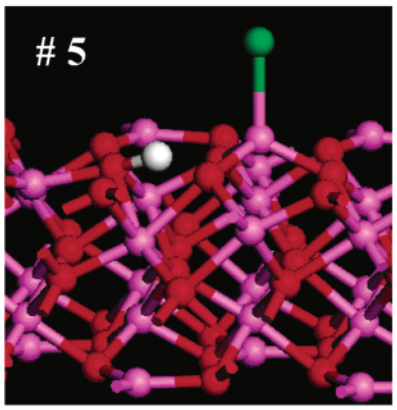

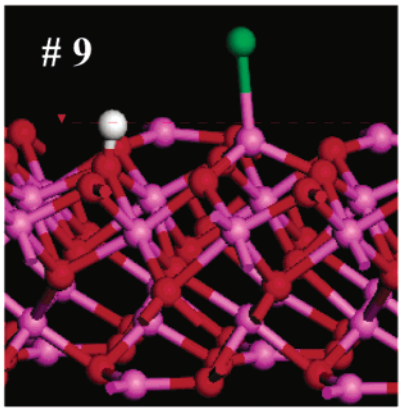

Figure 6. The energy profile for conversion of the 1−2 ionic state to the 1−4 ionic state of HCl adsorbed on the α-Al_2O_3 surface. A large activation barrier of ∼22 kcal/mol for the conversion is observed. The highest energy configuration along with the 1−2 and 1−4 ionic states are also shown. The high energy barrier shows that, at low temperatures, diffusion of the proton between the two ionic states will not occur.

For HCl adsorbed on the surface, the 1−2 dissociation product is substantially more stable than the 1−4 product (cf. Table 2). Both these products can be formed from the molecular precursor states with no activation barrier. The large energy barrier of ∼22 kcal/mol between the 1−2 and 1−4 sites (see Figure 6) precludes proton diffusion between neighboring sites, which in turn means that the Cl^- and H^+ will remain paired while adsorbed on the surface. This "pre-pairing" is consistent with the first-order kinetics observed in the TPD experiments.[7]

The energy difference between dissociated states of H_2O adsorbed on α-Al_2O_3(0001) is fairly small compared to that for the dissociative adsorption of HCl on that surface. Consequently, for H_2O the energy of both the initial molecular adsorbed state and the 1−2 and 1−4 dissociated products have the same energy to within 1 kcal/mol. The activation barrier for the formation of the 1−2 dissociation product is three times larger (6.6 as opposed to 2.2 kcal/mol) than that of the 1−4 dissociated product, so the kinetically preferred product of water dissociation is the 1−4 dissociated state.[11]

Adsorption at defective sites arising from missing oxygen atoms or near step edges has not been studied in this work. These will undoubtedly give different adsorption energies from those of a perfect surface.

Environmental Implications of the Adsorption of HCl on α-Al_2O_3. The reaction of HCl on the α-Al_2O_3 surface is considered to have important, practical environmental consequences. Large amounts of Al_2O_3 are released in the atmosphere during space shuttle and other rocket launches. The space shuttle booster rockets alone release more than 250 tons of aluminum oxide in the form of fine particles in the atmosphere per launch.[43] Experiments on different samples of rocket exhaust show that anywhere from 10 to 40% of the mass of aluminum oxide in the exhaust is in the form of α-Al_2O_3.[42] Hydrogen chloride is another major component of space shuttle exhaust, making up approximately 20% of its mass. Gas-phase reactions of HCl with many of the gas-phase participants of the ozone cycle are extremely slow but, when HCl adsorbs on the surface of ice particles in the polar stratospheric cloud, it has enhanced reactivity in reactions such as

$$ClONO_2(g) + HCl(s) \rightarrow HNO_3(s) + Cl_2(g) \qquad (7)$$

where the (s) denotes a surface adsorbed species. This is an indication that the mechanism involves ionic intermediates. Experimental[44−46] and theoretical[47−51] studies have been carried out on this reaction. Calculations of HCl on the ice surface[51] show that at least two H_3O^+ ions are required at the hexagonal ice surface sites in order for HCl to be ionized. Furthermore, molecular dynamics studies[51] show that Cl^- is mobile and can jump between neighboring hexagonal sites. The Cl^- on the ice surface is a strong nucleophile and may react with surface-adsorbed $ClONO_2$ by abstracting a Cl atom.[45] The chlorine gas produced in the reaction in eq 7 rapidly undergoes photodissociation to 2Cl, which catalyzes the conversion of O_3 to O_2. This is thought to be the most important active-chlorine-producing reaction in the stratosphere.[52]

It becomes apparent from our calculations that there are major differences between the adsorption of HCl on the α-alumina (0001) surface and on ice. In contrast to the pure ice surface, the strongly covalently bound HCl on alumina dissociates spontaneously to produce a pair of immobile Cl^- and H^+ ions. The covalently bonded Cl^- on alumina is a much weaker nucleophile, thus limiting its reactivity in the nucleophilic substitution reactions (chlorine abstractions) shown in eq 7. However, a water-covered α-alumina surface may enhance the reactivity of HCl.[53] The ionization of water on the surface will provide a local basic environment in which an adsorbed HCl

molecule can readily dissociate to Cl^-. There are no strong Lewis acid sites on the hydrated alumina surface and the Cl^- remains active in the Cl_2 producing reactions. There is experimental evidence for the production of active chlorine on the surface of H_2O-covered α-Al_2O_3 particles.[54] Preliminary studies[55] are being carried out on nanoparticles of Al_2O_3 with the Streitz−Mintmire potential.[20] A study of the charge distribution and local binding in these nanoparticles (of radius $\sim$ 40 Å) will give an indication of whether there are major differences in the binding modes of HCl to the nanoparticle as compared to the α-alumina (0001) surface.

5. Summary and Conclusions

We have demonstrated that plane-wave DFT calculations can be used to accurately reproduce the structural and energetic properties of bulk and (0001) surface of α-Al_2O_3 crystal and the chemisorption properties of HCl on this surface.

On the bare surface, the under-coordinated outermost layer of Al ions relaxes into the layer of O ions, drastically decreasing the separation between these layers from that in the bulk. The calculated distances in the relaxed surface is 0.02 Å compared to 0.84 Å in the bulk, a change of $\sim$97%. The effects of surface reconstruction extend further into the inner layers.

Upon adsorption of HCl onto the surface, the Al ion to which it attaches relaxes outward to a significant extent. The amount of relaxation depends on the binding mode of HCl to the surface. Adsorption of molecular HCl causes the surface Al ion to which it binds to relax outward, such that the vertical separation between the Al ion bound to the Cl of the molecule and the next layer of oxygen ions is −85% that of the bulk solid. The Al attached to the Cl^- that results from dissociative adsorption of HCl relaxes outward to an even greater extent. The distance between the Al−O planes are only between −14 and −20% that of the bulk solid. The exact distance between the planes depends on the specific configuration of H^+ and Cl^- on the surface.

Supercell slab model calculations show that even in the absence of surface imperfections and steps, there are a variety of adsorption sites available for HCl. Molecular HCl has an adsorption energy in the range of 14 kcal/mol and may be an important precursor to desorption. The results predict adsorption energies in the range of 35 to 45 kcal/mol when HCl dissociatively adsorbs. The different adsorption sites reflect the relative separation of H^+ and Cl^- on the surface.

The adsorption energy per HCl for dissociative adsorption decreases as the surface coverage on the 2×2 surface increases. This illustrates that repulsions are the dominant effect among the ions when H^+ and Cl^- ion pairs are adsorbed on adjacent sites and can explain why the observed saturation coverage is only 1/5 of the available surface Al sites.

Acknowledgment. This work was supported by Air Force Office of Scientific Research (Grant number F49620-00-1-0273) and the U.S. Army Research Office (Grant number DAAD19-01-1-0503).

References and Notes

(1) Henrich, V. E.; Cox, P. A. *The Surface Science of Metal Oxides*; Cambridge University Press:Cambridge, 1994.

(2) Noguera, C. *Physics and Chemistry at Metal Oxide Surfaces*; Cambridge University Press: Cambridge, 1996.

(3) Elam, J. W.; Nelson, C. E.; Cameron, M. A.; Tolbert, M. A.; George, S. M. *J. Phys. Chem. B* **1998**, *102*, 7008.

(4) Nelson, C. E.; Elam, J. W.; Cameron, M. A.; Tolbert, M. A.; George, S. M. *Surf. Sci.* **1998**, *416*, 341.

(5) Elam, J. W.; Nelson, C. E.; Cameron, M. A.; Tolbert, M. A.; George, S. M. *Surf. Sci.* **2000**, *450*, 64.

(6) Redhead, P. A. *Vacuum* **1962**, *12*, 203.

(7) Wise, M. L.; Koehler, B. G.; Gupta, P.; Coon, P. A.; George, S. M. *Surf. Sci.* **1991**, *258*, 166.

(8) Peri, J. B. *J. Phys. Chem.* **1966**, *70*, 1482.

(9) Tanaka, M.; Ogasawara, S. *J. Catal.* **1970**, *16*, 157.

(10) (a) Coustet, V.; Jupille, J. *Surf. Sci.* **1994**, *307−309*, 1161. (b) Coustet, V.; Jupille, J. *Nuovo Cimento D* **1996**, *19D*, 1657.

(11) Hass, K. C.; Schneider, W. F.; Curioni, A.; Anderoni, W. *J. Phys. Chem. B* **2000**, *104*, 5527.

(12) Lindblad, M.; Pakkanen, T. A. *Surf. Sci.* **1993**, *286*, 333.

(13) Wittbrodt, J. M.; Hase, W. L.; Schlegel, H. B. *J. Phys. Chem. B* **1998**, *102*, 6539.

(14) Dill, K. M.; Reed, R. A.; Calia, V. S.; Schulz, R. J. *J. Propul.* **1989**, *6*, 668.

(15) Wyckoff, R. W. G. *Crystal Structures*, 2nd ed.; Wiley: New York, 1964; Vol. 2, p 6.

(16) *International Tables for X-ray Crystallography, Vol. I.;* International Union for Crystallography; Kynoch Press: Birmingham, England, 1962.

(17) (a) Chang, C. C. *J. Appl. Phys.* **1968**, *39*, 5570. (b) Chang, C. C. *J. Vac. Sci. Technol.* **1971**, *8*, 500.

(18) French, T. M.; Somorjai, G. A. *J. Phys. Chem.* **1970**, *74*, 2489.

(19) Beitel, G. *Adsorption on Ordered Surfaces of Ionic Solids and Thin Films*; Freund, H.-J., Umbach, E., Eds.; Springer: Berlin, 1993; p 77.

(20) (a) Streitz, F. H.; Mintmire, J. W. *Phys. Rev. B* **1994**, *50*, 11996. (b) Keffer, D. J.; Mintmire, J. W. *Int. J. Quantum Chem.* **2000**, *80*, 733.

(21) (a) Campbell, T.; Kalia, R. K.; Nakano, A.; Vashishta, P.; Ogata, S.; Rodgers, S. *Phys. Rev. Lett.* **1999**, *82*, 4866. (b) Kalia, R. K.; Campbell, T. J.; Chatterjee, A.; Nakano, A.; Vashishta, P.; Ogata, S. *Computer Phys. Commun.* **2000**, *128*, 245.

(22) Manassidis, I.; De Vita, A.; Gillan, M. J. *Surf. Sci. Lett.* **1993**, *285*, L517.

(23) Ching, W. Y.; Xu, Y.-N. *J. Am. Ceram. Soc.* **1994**, *77*, 404.

(24) Kresse, G.; Hafner, J. *Phys. Rev. B* **1993**, *47*, 558; Kresse, G.; Hafner, J. *Phys. Rev. B* **1994**, *49*, 251.

(25) Kresse, G.; Furthmüller, J. *Comput. Mater. Sci.* **1996**, *6*, 15.

(26) Kresse, G.; Furthmüller, J. *Phys. Rev. B* **1996**, *54*, 11169.

(27) Vanderbilt, D. *Phys. Rev. B* **1990**, *41*, 7892.

(28) Kresse, G.; Hafner, J. *J. Phys. Condens. Matter* **1994**, *6*, 8245.

(29) Monkhorst, H. J.; Pack, J. D. *Phys. Rev. B* **1976**, *13*, 5188.

(30) Perdew, J. P.; Wang, Y. *Phys. Rev. B* **1992**, *45*, 13244.

(31) Perdew, J. P.; Chevary, J. A.; Vosko, S. H.; Jackson, K. A.; Pedersen, M. R.; Singh, D. J.; Frolhais, C. *Phys. Rev. B* **1992**, *46*, 6671.

(32) Kresse, G.; Hafner, J. *Phys. Rev. B* **1993**, *47*, 558.

(33) Jónsson, H.; Mills, G.; Jacobsen, K. W. Nudged elastic band method for finding minimum energy paths of transitions. In *Classical Quantum Dynamics in Condensed Phase Simulations*; Berne, B. J., Ciccotti, G., Coker, D. F., Eds.; World Scientific: Singapore, 1998; p 385.

(34) Anderson, D. L. *Theory of the Earth*; Blackwell Scientific Publications: Boston, 1989.

(35) Goto, T.; Anderson, O. L.; Ohno, I.; Yamamoto, S. *J. Geophys. Res. (Solid Earth Planets)* **1989**, *94*, 7588.

(36) *CRC Handbook of Chemistry and Physics*, 67th ed.; CRC: Boca Raton, Fl., 1983.

(37) (a) Guenard, P.; Renaud, G.; Barbier, A.; Gautier-Soyer, M. *Mater. Res. Soc. Symp. Proc.* **1996**, *437*, 15. (b) Ahn, J.; Rabalais, J. W. *Surf. Sci.* **1997**, *338*, 441.

(38) (a) Mackrodt, W. C. *J. Chem. Soc., Faraday Trans. 2* **1989**, *85*, 541. (b) Mackrodt, W. C.; Davey, R. J.; Black, S. W.; Docherty, R. *J. Cryst. Growth* **1987**, *80*, 441.

(39) Tasker, P. W. *Adv. Ceram.* **1988**, *10*, 176.

(40) Huber, K. P.; Herzberg, G. *Molecular Spectra and Molecular Structure, Vol. IV, Constants of Diatomic Molecules*; Van Nostrand: New York, 1979.

(41) Graybeal, J. D. *Molecular Spectroscopy*; McGraw-Hill: New York, 1988.

(42) Dill, K. M.; Reed, R. A.; Calia, V. S.; Schulz, R. J. *J. Propul. Power* **1990**, *6*, 668.

(43) Cofer, W. R., III.; Garland Lala, G.; Wightman, J. P. *Atmos. Environ.* **1987**, *21*, 1187.

(44) Lee, S.-H.; Leard, D. C.; Zhang, R.; Molina, L. T.; Molina, M. J. *Chem. Phys. Lett.* **1999**, *315*, 7.

(45) Horn, A. B.; Sodean, J. R.; Roddis, T. B.; Williams, N. A. *J. Phys. Chem. A* **1998**, *102*, 6107.

(46) Oppliger, R.; Allanic, A.; Rossi, M. J. *J. Phys. Chem. A* **1997**, *101*, 1903.

(47) (a) Bianco, R.; Hynes, J. T. *J. Phys. Chem. A* **1999**, *103*, 3797. (b) McNamara, J. P.; Tresadern, G.; Hillier, I. H. *J. Phys. Chem. A* **2000**, *104*, 4030.

(48) Toubin, C.; Picaud, S.; Hoang, P. N. M.; Girardet, C.; Demirdijan, B.; Ferry, D.; Suzanne, J. *J. Chem. Phys.* **2002**, *116*, 5150.

(49) Mantz, Y. A.; Geiger, F. M.; Molina, L. T.; Molina, M. J.; Trout, B. L. *J. Phys. Chem.* **2001**, *105*, 7037.

(50) Mantz, Y. A.; Geiger, F. M.; Molina, L. T.; Molina, M. J.; Trout, B. L. *Chem. Phys. Lett.* **2001**, *348*, 285.

(51) Svanberg, M.; Pettersson, J. B. C.; Bolton, K. *J. Phys. Chem. A* **2000**, *104*, 5787.

(52) Seinfeld, J. H.; Pandis, S. N. *Atmospheric Chemistry and Physics*; Wiley: New York: 1998.

(53) Nelson, C. E.; Elam, J. W.; Tolbert, M. A.; George, S. M. *Appl. Surf. Sci.* **2001**, *171*, 21.

(54) Molina, M. J.; Molina, L. T.; Zhang, R.; Meads, R. F. *Geophys. Res. Lett.* **1997**, *24*, 1619.

(55) Alavi, S.; Thompson, D. L. Unpublished results.